nature materials

ARTICLES

PUBLISHED ONLINE: 19 AUGUST 2012 | DOI: 10.1038/NMAT3402

Deep-subwavelength imaging of the modal dispersion of light

R. Sapienza[1,2]*, T. Coenen[3], J. Renger[1], M. Kuttge[1], N. F. van Hulst[1,4] and A. Polman[3]

Numerous optical technologies and quantum optical devices rely on the controlled coupling of a local emitter to its photonic environment, which is governed by the local density of optical states (LDOS). Although precise knowledge of the LDOS is crucial, classical optical techniques fail to measure it in all of its frequency and spatial components. Here, we use a scanning electron beam as a point source to probe the LDOS. Through angular and spectral detection of the electron-induced light emission, we spatially and spectrally resolve the light wave vector and determine the LDOS of Bloch modes in a photonic crystal membrane at an unprecedented deep-subwavelength resolution (30–40 nm) over a large spectral range. We present a first look inside photonic crystal cavities revealing subwavelength details of the resonant modes. Our results provide direct guidelines for the optimum location of emitters to control their emission, and key fundamental insights into light–matter coupling at the nanoscale.

The LDOS is a key fundamental quantity involved in light–matter interaction, as it provides a direct measure for the probability of spontaneous light emission[1] and light scattering[2,3]. Recent advances in nanostructuring of photonic materials have allowed tailoring of the LDOS at the nanoscale, thereby enabling many new applications in lighting, displays, light management in solar cells, quantum optics and information technology. Light–matter coupling, either to the far field or to well-defined optical modes, is maximized when the source is placed at a position where the LDOS is highest. Key demonstrations of this effect are, for example, the enhanced spontaneous emission of quantum dots in the field maximum of a photonic crystal cavity[4,5] or the directional emission in the proximity of a metallic nanoantenna[6].

Photonic crystals are key geometries that have been studied for many years in this respect, as they provide full control over the dispersion of light by engineering the momentum of light $\mathbf{k}(\omega)$. Furthermore, photonic crystal cavities[7] have shown strong confinement of light, leading to nanoscale on-chip lasers, light-emitting diodes and platforms to probe the quantum interaction between light and matter[8]. In a photonic crystal the subwavelength scale modulation of the dielectric constant results in large spatial and frequency variations of the LDOS, corresponding to either strongly inhibited or enhanced light emission at well-defined emitter locations and frequencies. A full understanding of light–matter interaction requires the mapping of the LDOS $\rho(\mathbf{r}, \mathbf{k}, \omega)$ in space, momentum and frequency. So far, most methods to determine the LDOS are based on measurements of the modification of the spontaneous emission rate of optical emitters (the Purcell effect). According to Fermi's golden rule the fluorescence decay rate Γ of a single dipole is proportional to the position- and frequency-dependent LDOS $\rho_{\hat{\mathbf{p}}}(\mathbf{r}, \omega)$, projected onto the dipole direction $\hat{\mathbf{p}} = \mathbf{p}/|\mathbf{p}|$. Spatially resolved LDOS measurements using this technique require scanning a moveable probe with an optical emitter at its end, such as a fluorescent dye[9], a diamond nanocrystal[10] or a polymer sphere[11], over the optical modal landscape while measuring its fluorescence decay. Pioneering LDOS maps have been recently achieved in this way[11]. Alternatively, in the reciprocal configuration, the photonic structure can be scanned over a fixed dipole emitter. In the last method, the LDOS near metallic nanoantennas[12] and photonic crystals[13] has been probed. Conventional passive near-field scanning optical microscopy can also be used to map the LDOS (refs 14–16), but it is restricted to the momentum collected by the tip, and to the spatial resolution of the physical size of the tip aperture of ∼100 nm. Major disadvantages of the LDOS scanning probe techniques include that they are experimentally challenging, slow and limited by the narrow spectral width, and photobleaching of the light source. Moreover, the fluorescent probe itself potentially affects the LDOS landscape. More importantly, whereas all of the above techniques focus on the spatial dependence of the LDOS, they ignore an equally important aspect of local mode imaging, that is, the determination of the local momentum of light. By collecting the angle-resolved emission spectrum, and thus determining the in-plane wave vector of the emitted light, a wealth of information regarding the photonic band structure and the nature of local modes can be collected[17]. Together, despite numerous experimental efforts, an accurate broadband, non-invasive technique to determine the LDOS and optical momentum distribution in two-dimensional photonic structures at deep-subwavelength resolution is still elusive.

Here, we use a scanning electron beam as a point dipole source to probe the LDOS in space, frequency and momentum. Compared with usual fluorescent probes, the created cathodoluminescence probe exhibits a broad spectral range, precise localization down to 30–40 nm and no bleaching, therefore allowing us to record high-resolution LDOS maps and reconstruct the optical momentum distribution. Cathodoluminescence originates from the coupling of a high-energy electron's external field to the local modes of a photonic structure. This leads to the generation of cathodoluminescence in the form of transition radiation when the electron crosses an interface or Cherenkov radiation when it moves faster than the speed of light in a medium[18]. The energy and momentum required to excite cathodoluminescence are provided by the kinetic energy and momentum of the electron, and correspond to a very broad

[1]ICFO-Institut de Ciencies Fotoniques, Mediterranean Technology Park, 08860 Castelldefels (Barcelona), Spain, [2]Department of Physics, Kings College London, Strand, London WC2R 2LS, UK, [3]Center for Nanophotonics, FOM Institute AMOLF, Science Park 104, 1098 XG Amsterdam, The Netherlands, [4]ICREA-Institució Catalana de Recerca i Estudis Avançats, 08015 Barcelona, Spain. *e-mail: riccardo.sapienza@kcl.ac.uk.

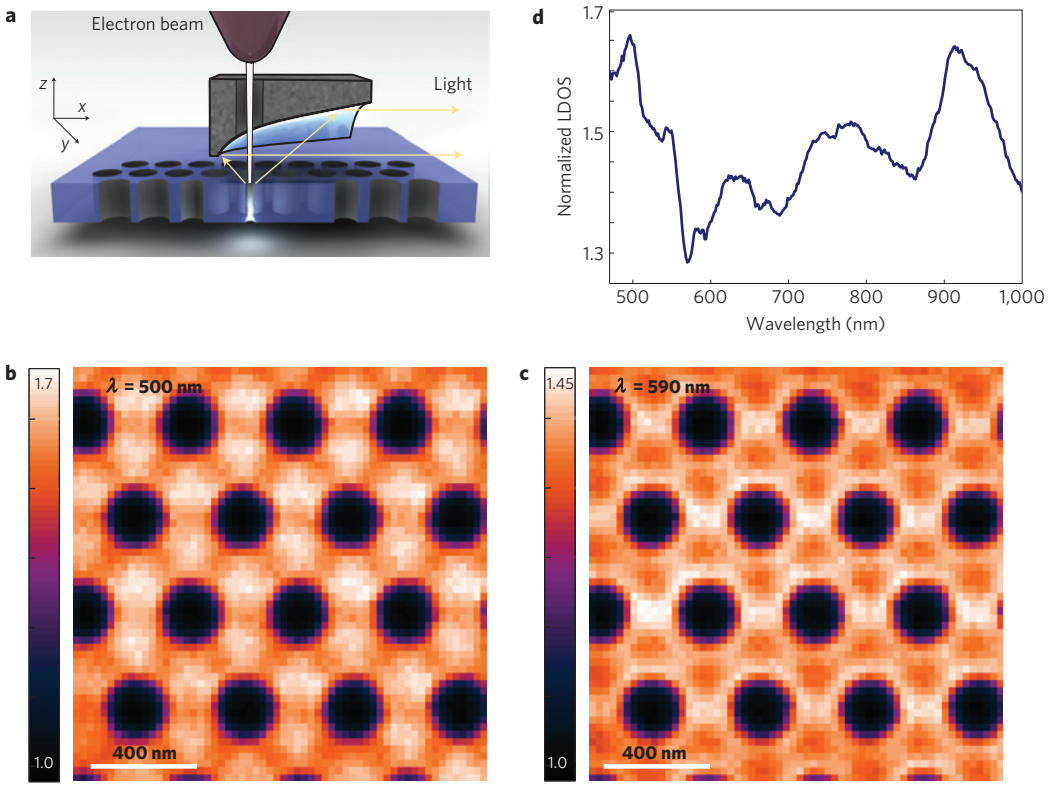

Figure 1 | High-resolution LDOS mapping on two-dimensional photonic crystals. a, Sketch of the experimental set-up: an electron beam is incident on the sample surface, generating optical radiation that is collected by the mirror placed above the sample and sent to an optical spectrometer or to an imaging CCD (charge-coupled device) camera. Scanning of the electron beam allows for deep-subwavelength spatial mapping of the LDOS. **b**,**c**, LDOS maps of a photonic crystal Si_3N_4 membrane with a lattice constant $a = 400$ nm and a hole diameter of 230 nm in the high-energy bands at a wavelength of 500 nm ($a/\lambda = 0.8$) and 590 nm ($a/\lambda = 0.68$), respectively. The Bloch mode is visible in its periodic LDOS modulation, it is delocalized over the full crystal and has the same symmetry as the lattice. **d**, LDOS spectrum taken in the centre between three holes, normalized by the cathodoluminescence emission from an unstructured membrane reference. The Bloch modes modulate the LDOS by 30%. The LDOS maps are the raw data without any background subtraction, corrected only for system response and are integrated over a 9 nm bandwidth.

excitation spectrum ranging from the ultraviolet to the far-infrared. In practice, the interaction of the electron with the medium can be represented by a transient dipole aligned along the electron trajectory and placed at the electron impact position (transition radiation) or along the electron path (Cherenkov radiation). For a given material, this transient dipole has a constant amplitude but importantly the power dissipated by the electron depends on its local photonic surrounding. This way, it is sensitive to the optical mode density at the impact location[18] and its radiated power is given by $P = (\pi\omega^2)/(12\epsilon_0)\,|\mathbf{p}|^2\,\rho_{\hat{\mathbf{p}}}(\mathbf{r},\omega)$, where $\mathbf{p}$ is the dipole moment of the induced dipole, ϵ_0 is the surrounding dielectric constant and $\rho_{\hat{\mathbf{p}}}(\mathbf{r},\omega)$ is the radiative part of the projected LDOS. A measurement of the total radiated emission would then directly probe the LDOS $\rho_{\hat{\mathbf{p}}}(\mathbf{r},\omega)$. More precisely, at 30 keV electron energy, the observed light emission is a measure of the LDOS component projected onto a single direction along the electron trajectory, which is the direction of the transient dipole[19]. One clear demonstration of this is the fact that angle-resolved measurements of cathodoluminescence on a planar Au surface show a radiation pattern that is identical to that of a z-oriented point dipole placed at the Au surface[20]. Moreover, the obtained intensity is a measure of the radiative component of the LDOS, completely unaffected by non-radiative decay channels, in contrast to standard optical probe methods, demonstrating the only technique to our knowledge that probes a pure vectorial component of the radiative LDOS.

So far, cathodoluminescence spectroscopy has mostly been used to investigate optical modes in metallic nanostructures such as nanoparticles and nanodiscs where it excites either local dipolar or higher-order modes[17,21–24]. Here, we demonstrate the excitation, by the electron beam, of Bloch modes and localized modes in a two-dimensional dielectric photonic crystal. In the experiment, a 30 keV electron beam is scanned over the surface of a hexagonal photonic crystal composed of holes in a 200-nm-thick Si_3N_4 membrane (refractive index $n \simeq 2.0$) supported by a Si wafer. At every electron beam position, the emitted light spectrum is collected using a parabolic mirror placed between the sample and the microscope pole piece (Fig. 1a) and a two-dimensional map of the photonic crystals LDOS $\rho_{r,\hat{z}}(x,y)$ is recorded. Momentum spectroscopy is carried out by collecting the angular distribution of the emitted light at precise electron beam positions on the photonic crystal.

Figure 1b,c shows LDOS images of the photonic crystal with a lattice constant of $a = 400$ nm and a hole diameter of 230 nm, at collection wavelengths of 500 and 590 nm. These wavelengths correspond to frequencies above the first bandgap for this photonic crystal ($a/\lambda = 0.8$ and 0.68, respectively, with a being the lattice constant). The periodic pattern of holes is clearly visible as the dark circles at which no emission is excited. The image clearly shows that the modes are fully delocalized over the photonic crystal with the periodicity of the photonic crystal unit cell. The LDOS images are very distinct for the two wavelengths, with LDOS hotspots observed in the triangular regions between the holes for $\lambda = 500$ nm and LDOS maxima around the hole circumferences for $\lambda = 590$ nm. Distinct LDOS patterns clearly reflect the quasi-orthogonality of the photonic crystal eigenmodes at different frequencies. Figure 1d shows the cathodoluminescence spectrum taken at the symmetry point between three holes. The modal peaks

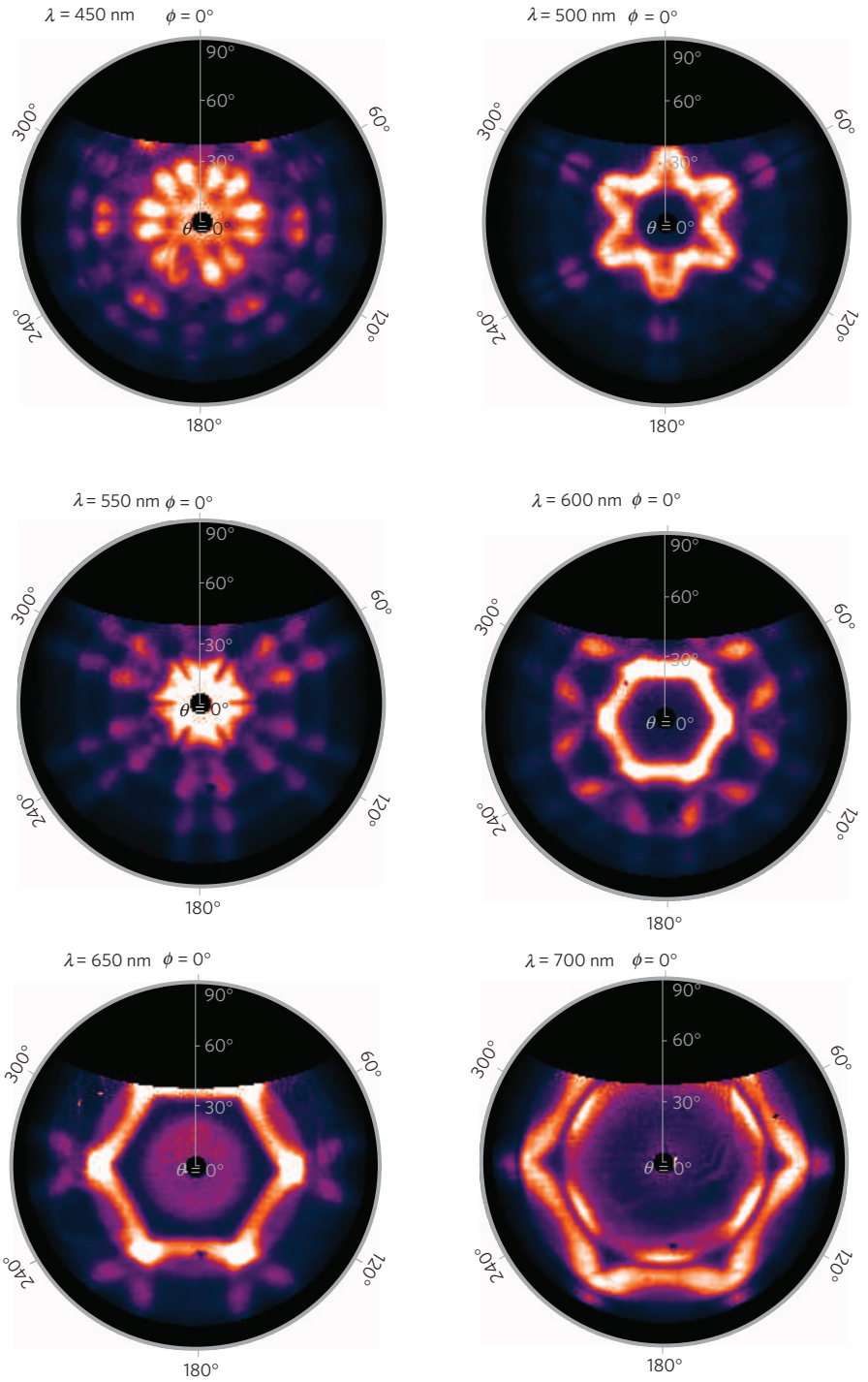

Figure 2 | Momentum spectroscopy of a two-dimensional photonic crystal. Angular emission patterns from a photonic crystal at different wavelengths (collected bandwidth ~40 nm) by exciting the photonic crystal in the symmetry point between three holes. The images at a wavelength of 500 and 600 nm correspond to the spatial LDOS maps in Fig. 1b,c. Azimuthal (ϕ) and polar (θ) angles are indicated. The hexagonal symmetry is clearly visible as well as an increasing number of polar peaks for higher energies. The black area at the top and the black circle in the centre of the images correspond to angular ranges that are not collected by the mirror.

at 500 and 590 nm are clearly visible in the spectrum. The maximum LDOS variation observed across the images in Fig. 1b,c is ~30% of the average value.

Momentum spectroscopy at various wavelengths, by exciting the photonic crystal in the symmetry point between three holes, is presented in Fig. 2. Complex angular emission patterns are observed for the photonic crystal with a hexagonal symmetry as expected. As in the spatial maps of Fig. 1b,c, very distinct patterns are observed for the two wavelengths of 500 and 600 nm (collected bandwidth ~40 nm), reflecting the different modal distributions. The momentum spectroscopy maps are portions of the isofrequency surfaces, plotting the allowed $\mathbf{k}$ at a given ω: dark areas correspond to forbidden in-plane momenta in the crystal, whereas bright peaks correspond to the in-plane momentum of photonic crystal eigenmodes[25]. Momentum spectroscopy provides key information beyond just the band diagram, as it probes

the momentum of light at all angles and not only along the symmetry directions, and could thus be very useful to study negative refraction, self-collimation and light localization in both periodic and aperiodic systems.

Even larger LDOS variations can be achieved with a localized mode in a photonic crystal cavity. Figure 3a shows a scanning electron microscope (SEM) image of a single-hole defect (H1) cavity in a photonic crystal with a lattice period of $a = 330$ nm and a hole diameter of 230 nm. In Fig. 3b the LDOS image is taken at a wavelength of $\lambda = 650$ nm ($a/\lambda = 0.51$), corresponding to the cavity resonance frequency inside the photonic bandgap. At this wavelength, the image shows a strongly confined localized mode inside the cavity. The LDOS is imaged with unparalleled resolution, here revealing features of ~70–80 nm width, with a spatial resolution of 30–40 nm (see below). A LDOS hotspot is observed at the cavity centre, and further maxima are observed on either side of the six hexagonal spokes extending outwards. Momentum spectroscopy for this cavity is shown in Fig. 3c by exciting the cavity in the centre. A hexagonally shaped angular emission pattern is observed, with a dominant maximum for emission normal to the sample, corresponding to zero in-plane momentum (the black spot in the centre for $\theta < 5°$ is due to the hole in the mirror). These are the k components of a localized mode with a large k distribution[26]. k-space engineering, and in particular suppression of the k components close to $k = 0$ that couple to the light cone, is one of most important techniques to increase the Q value of photonic crystal cavities[27]. Figure 3c also shows a weaker emission band around a polar angle of $\theta = 45°$. This band is also observed in the angular pattern measured on an unstructured Si_3N_4 membrane (Fig. 4f) and is attributed to the interference of light emitted from the top and bottom of the membrane, the latter being reflected upwards by the Si substrate 1 μm below the membrane.

Figure 4a,b shows the LDOS maps for a larger photonic crystal cavity composed of a linear three-hole (L3) defect. Data are taken at two wavelengths corresponding to the two resonant modes observed in the LDOS spectrum of Fig. 4c. The LDOS distributions of the two modes are very distinct and reflect their quasi-orthogonality. At $\lambda = 649$ nm spatially narrow LDOS hotspots are observed around the inner cavity edges near the holes, whereas at 681 nm three LDOS hotspots are observed near the positions of the three missing holes. In the latter hotspots the LDOS is increased by a factor of 2 as compared to an unstructured membrane. This corresponds well to the value calculated from the Purcell formula $\rho_{max}(\omega) = 3/4\pi^2\,(\lambda/n)^3 \times Q(\omega)/V_{eff} = 1.9$, assuming a mode volume V_{eff} of $0.7\,(\lambda/n)^3$ and $Q(\omega) \sim 10$ derived from the linewidth of the resonances, obtained from the half-profile of the spectral peak at 681 nm in the LDOS spectrum (Fig. 4c). These low Q values are expected as out-of-plane dipoles experience a much weaker cavity than in-plane ones, for which the bandgap is maximized in a membrane geometry. Further spectral measurements performed at lower electron energy (5 keV) indicate the probing of x, y and z LDOS components, with stronger coupling to in-plane directions, revealing sharper and higher peaks (see Supplementary Information). Numerical calculations, performed by three-dimensional finite-difference time-domain methods, of LDOS spectral maps are presented in Fig. 4g–i. The experimental spectral peaks in Fig. 4c are differently shaped than in the theoretical curve in Fig. 4i, which we attribute to a small mismatch between the simulated and measured geometry. The spatial maps in Fig. 4g,h show the same symmetry and similar LDOS distributions as the measured ones in Fig. 4a,b. Clearly, these high-resolution LDOS maps provide a direct guideline for the optimum locations at which emitters at a certain wavelength would be coupled to the corresponding cavity mode. The momentum spectroscopy maps for the two cavity modes are shown in Fig. 4d,e for the two resonance frequencies. These data are taken by positioning the electron beam

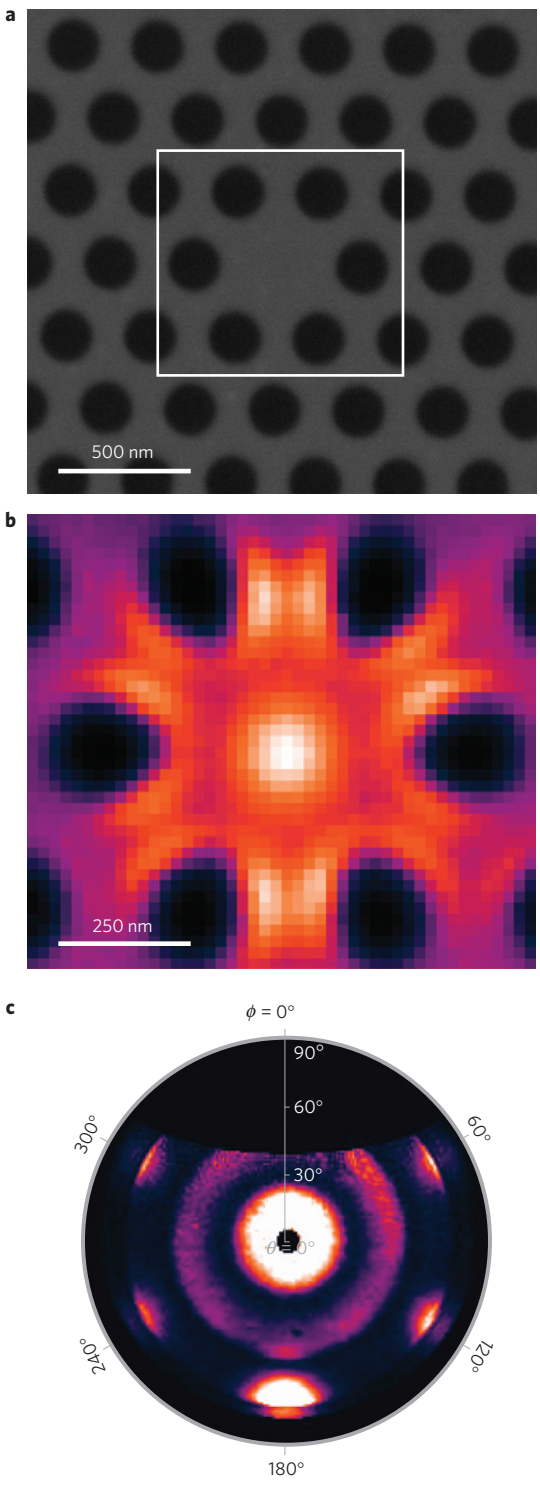

Figure 3 | LDOS maps and momentum spectrum of a H1 photonic crystal cavity. a, Secondary electron microscopy image of a photonic crystal membrane with a hole defect (H1 cavity) with a lattice constant $a = 330$ nm and a hole diameter of 230 nm. The area outlined is shown in **b**. **b**, LDOS image of the cavity at a wavelength of 650 nm, with a bandwidth of 9 nm. **c**, Angular emission pattern when the cavity is excited in its centre (collection bandwidth ~40 nm). The hexagonal momentum distribution shows a maximum around $k = 0$ and a hexagonal pattern of lobes.

at a LDOS maximum corresponding to each distinct mode. The more complex nature of these cavity modes, compared with the H1 cavity in Fig. 3, is directly reflected in the angular emission maps. A

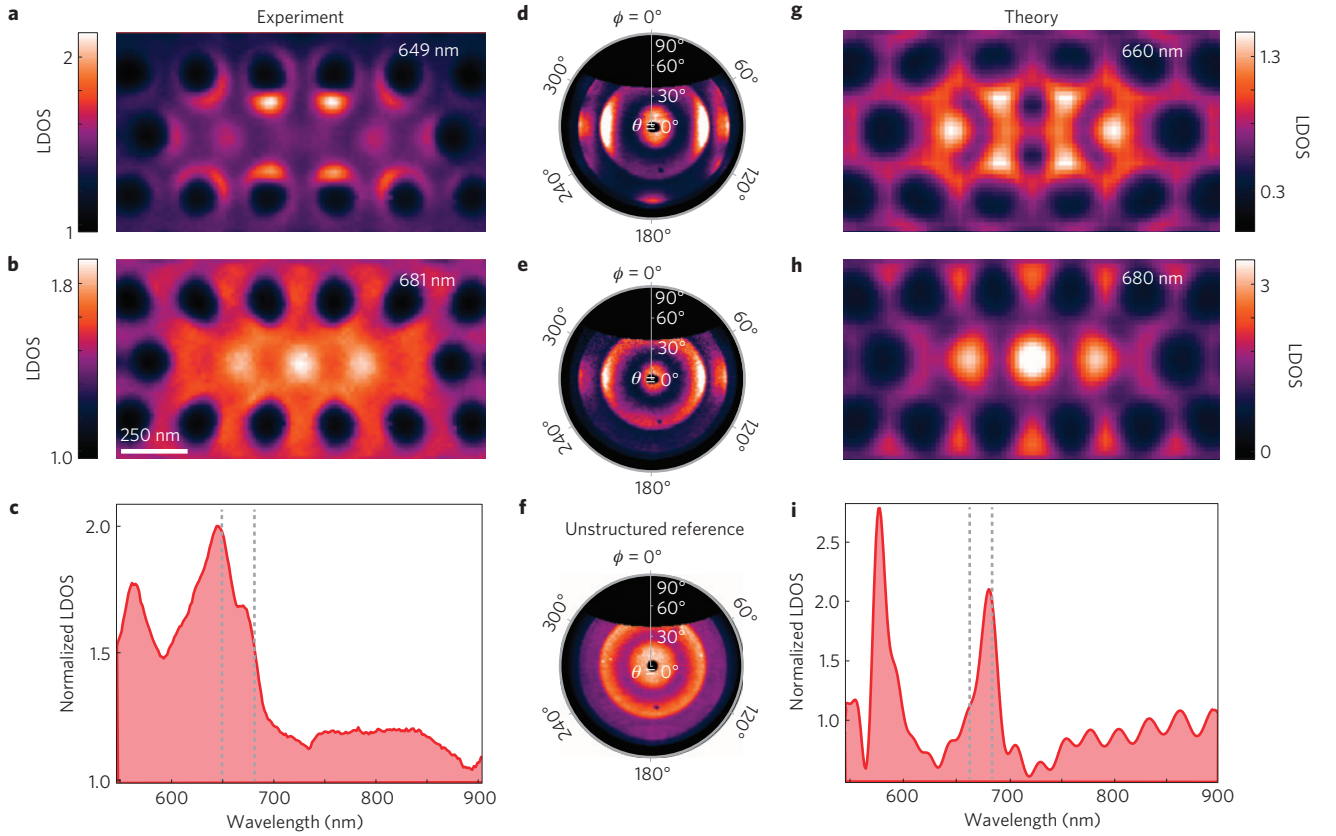

Figure 4 | Mapping multiple cavity modes of an L3 photonic crystal cavity. a,**b**, Measured LDOS maps of an L3 photonic crystal cavity (lattice period $a = 330$ nm, hole diameter $d = 230$ nm) at the frequency of the two cavity modes, 649 and 681 nm, respectively, with a bandwidth of 9 nm. **c**, Measured cavity resonance spectrum measured in the centre of the cavity normalized to the spectrum of an unstructured membrane. The cavity modes exhibit an increase of LDOS of a factor of ~2 at the resonance location. **d**,**e**, Measured angular emission patterns at the two resonance frequencies. The long axis of the cavity is parallel to the horizontal direction along 90° and 270°. The cavities exhibit clear directional emission peaks, at 90° and 270° for both wavelengths. **f**, The vague circular pattern in the background is attributed to the interference of light emitted from the cavity with light reflected by the silicon substrate, as also observed for a reference unstructured membrane. **g**,**h**, Calculated LDOS maps for the same experimental parameters (see Methods). The theoretical maps exhibit the same symmetry and similar LDOS distribution as in the experiments. **i**, The LDOS spectra calculated in the middle of the cavity; two peaks are visible, at around 600 and 680 nm. The vertical dotted lines in **c** and **i** indicate the position of the LDOS maps shown above.

strong asymmetry in the emission is observed, with intense lobes at azimuthal angles $\phi = 90°$ and 270°, peaking at a polar angle around $\theta \sim 53°$. This emission is attributed to the constructive interference of radiation emitted from the linear cavity in the far field, in a way similar to what is observed for standing waves along metallic wire antennas[28,29].

The resolution of the LDOS imaging technique is determined by the spot size of the electron beam and the radial extent of the evanescent field around the electron beam trajectory. The first is determined by the electron optics of the electron microscope, and is 1–10 nm for a typical SEM. For cathodoluminescence, to increase the signal-to-noise ratio and avoid nanoscale sample drift during the measurement, it is advantageous to use a relatively high beam current (10 nA), in which case the electron beam spot diameter is about 10 nm. The radial extent of the field around the electron beam trajectory is given by:

$$\mathbf{H}_j^{\mathrm{bulk}}(\mathbf{r},\omega) = -\frac{2e\omega}{v c\gamma} e^{i\omega z/v} K_1\left(\frac{\omega\rho}{\gamma v}\right)\hat{\phi} \qquad (1)$$

where ρ is the distance from the electron trajectory, z is the position along the trajectory, e is the electron charge, ω is the frequency, v is the electron velocity, c is the speed of light in vacuum, $\gamma = 1/\sqrt{1-v^2/c^2}$ is the Lorentz contraction factor, $\hat{\phi}$ is the azimuthal unit vector and K_1 is the modified Bessel-function of the second kind. Details of the derivation of equation (1) are given in ref. 18. Equation (1) is a diverging function for $\rho = 0$, and thus represents a very high potential spatial resolution. Taking into account the delocalized character of the material response, an upper limit of the resolution is given by the $1/e$ decay distance ($v\gamma/2\omega$) of the K_1 function in equation (1). For a perfectly focused 30 keV electron beam, this corresponds to a $1/e$ distance of 17 nm at a wavelength of 600 nm (ref. 30). A corresponding Gaussian function has $\sigma = 11$ nm and a full-width at half-maximum (FWHM) of 26 nm. For a perfectly focused electron beam, the LDOS resolution at 30 keV thus is <26 nm. For a typical electron beam spot diameter of 10 nm FWHM, the theoretical spatial resolution then is <36 nm, depending on the electron beam profile.

To measure the spatial resolution in our set-up we measured the cathodoluminescence intensity along a sharp edge between a Si membrane and air and compared it to the SEM image taken in the same scan. Figure 5a shows the cathodoluminescence intensity at wavelengths in the range 500–900 nm along a line scanned across a 150 nm square hole in a Si membrane, whose SEM image is shown in Fig. 5c. Figure 5b (open dots) shows a line-scan of the cathodoluminescence intensity at a wavelength of 600 nm. The signal from a single hole is dominated by the transition radiation

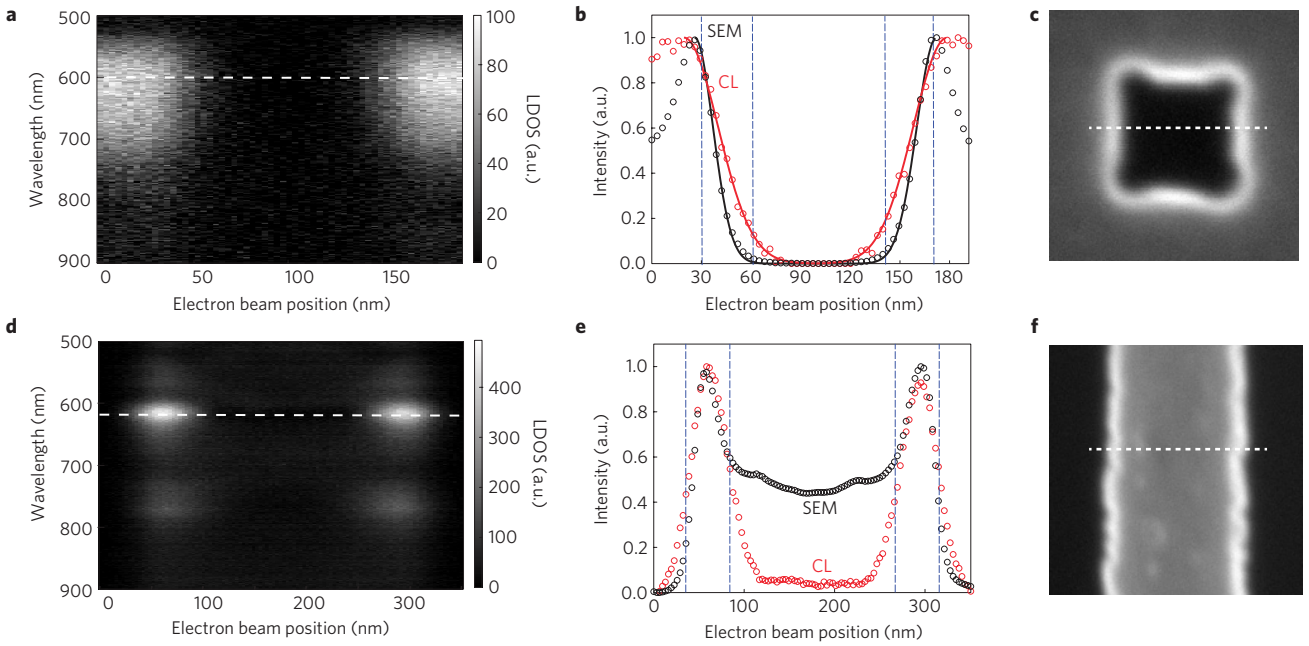

Figure 5 | Resolution assessment. a–c Line-scans over a 150 nm square hole in a silicon membrane. **b** shows the line-cut of the LDOS at the wavelength of 600 nm as compared with the SEM topology line-cut. CL, cathodoluminescence. The LDOS signal drops from 10% to 90% in 33 nm, following the topology, which drops from 10% to 90% in 21 nm. **d–f**, Plots of the measurements performed on the opposite geometry of a silicon membrane nanostrip. Such a system supports sharp spectral resonances that are spatially localized at the edges of the strip. These sharp features are compared in **e** to the SEM topology image. Their width at half-maximum is 48 nm. In **b**,**e** the open dots are the measured data, and the solid lines are the result of the fit. The blue vertical lines show the 90–10% signal drop. In **a**,**c**,**d**,**f** the white dotted line shows the spectral and spatial position of the line-cut. Measurements were made using 3 nm steps in the electron beam position.

at the boundary between vacuum and silicon, where the LDOS is increased. In the visible range we do not observe a clear spectral peak signature of a dielectric hole resonance. The cathodoluminescence signal shows a sharp transition at the edge, decreasing from 90% to 10% over a distance of 33 nm. Fitting a Heaviside step function with a Gaussian resolution function on both edges (solid line) we find an average standard deviation (s.d.) in the cathodoluminescence measurement of $\sigma_{CL} = 21$ nm. This measured value thus provides an upper limit of the s.d. of the LDOS resolution. It is determined by the electron beam spot size, the effective width of the edge and the evanescent extent of the field around the electron beam trajectory. The first two terms can be estimated from a line-scan of the secondary electron signal across the edge, which is also shown in Fig. 5b: the corresponding s.d. is $\sigma_{SEM} = 11$ nm. Deconvoluting the two signals we find the electron beam interaction width to be represented by a s.d. of $\sigma = 13$ nm, close to the theoretical value of $\sigma = 11$ nm. This value corresponds to a FWHM of the corresponding Gaussian distribution of 30 nm. Taking into account the electron beam spot diameter of ~10 nm the resolution then is 30–40 nm, depending on the electron beam profile. The measured value is in excellent agreement with the theoretical resolution of <36 nm calculated above.

To illustrate that the width of features in cathodoluminescence scans is most often determined by the physical width of the LDOS profile, we measured the cathodoluminescence signal across a narrow free-standing 200-nm-wide, 200-nm-thick Si strip, made using electron-beam lithography and etching of a free-standing Si membrane. This structure acts as a nanoscale Fabry–Perot cavity with a first-order resonance at 620 nm, determined by the strip width and refractive index. Figure 5d shows the result of the spectral LDOS measurement. The sharp resonance leads to a strongly enhanced LDOS at the resonance field maxima at the end facets of the cavities, as is clearly seen in Fig. 5d. A line-scan through these sharp features is shown in Fig. 5e together with a line-scan through the corresponding secondary electron intensity (Fig. 5f). The FWHM of the cathodoluminescence peaks is 48 nm. Given that the spatial resolution of cathodoluminescence is 30–40 nm (see above), this width is also determined by the width of the LDOS profile of the resonant mode on the Si strip. Similarly, the narrowest features in the LDOS measurements on the Si_3N_4 membrane in Fig. 4a, close to the hole edges, have a FWHM of ~70 nm, again limited by the physical width of the LDOS profile.

The LDOS imaging we present here, like all spectroscopic techniques, has some limits. LDOS can be probed only in a polarizable medium and not in, for example, the holes of the photonic crystal. The analysis presented here is made for planar samples, for which the electron beam is incident normal to their surface, and so far an extension to three dimensions is lacking. Exotic emission components propagating close to the sample surface could escape the numerical aperture of the detection and therefore their contribution would be underestimated. Last, high-quality LDOS measurements require a (weakly) conducting non-luminescent substrate such as Si or Si_3N_4 to prevent sample charging on electron beam irradiation as well as unwanted optical transitions that could blur the LDOS features.

We have resolved the LDOS $\rho_{r,\hat{z}}(x, y, \omega, \mathbf{k})$ in a two-dimensional photonic crystal in the spatial, spectral and momentum domain using cathodoluminescence imaging spectroscopy. We demonstrate a deep-subwavelength resolution of 30–40 nm and background-free detection, in addition to angle-resolved detection capabilities that provide high-resolution momentum imaging. We provide high-resolution images of the propagating Bloch modes in the photonic crystal at frequencies above the photonic bandgap. In addition, we directly probe the modal distribution of localized modes inside photonic crystal defect cavities, measured at frequencies inside the bandgap. Momentum spectroscopy reveals the wave vectors for the propagating Bloch modes and confirms the nature of the localized modes. This work demonstrates that the angle-resolved

cathodoluminescence technique is a very powerful method to resolve the photonic density of states locally in dielectric materials and may enable a wealth of further studies on light propagation and localization in complex photonic systems.

Methods

Set-up. The cathodoluminescence experiment was performed in an FEI XL-30 SFEG scanning electron microscope with a diamond-turned aluminium paraboloid mirror inside, with a numerical aperture of 0.96. The mirror alignment is accomplished using a piezoelectric positioning system. This paraboloid has a 600-μm-diameter hole directly above its focal point, through which a 30 keV electron beam can reach the sample. The emitted radiation is collected by the mirror and redirected out of the SEM through a glass vacuum flange. For spectral imaging the radiation was focused onto a fibre leading to a spectrometer with a liquid-nitrogen-cooled CCD (charge-coupled device) array.

For the momentum spectroscopy, the angular measurements are obtained by projecting the Fourier plane of the sample surface onto a 1,024 × 1,024 imaging CCD array. Each pixel of the CCD camera corresponds to a unique combination of polar (θ) and azimuthal (ϕ) angles. For angular measurements the electron beam energy has been set to 5 keV to achieve best contrast, inducing a partial mixing of *xyz* components (see Supplementary Information). All measurements were performed at room temperature. More details of the set-up can be found in ref. 19. The typical photon collection rate integrated over all of the wavelength range collected by the cooled CCD detector is, at 30 keV, $\sim 10^{-3}$ photons per electron.

Sample. The photonic crystals have been made by structuring a poly(methyl methacrylate) resist by electron-beam lithography followed by reactive ion-etching of the Si_3N_4 membrane. The 200-nm-thick membrane was spaced 1,000 nm from the silicon substrate by a sacrificial silica layer that has been removed using hydrofluoric acid etching. The samples used for the assessment of the resolution were made in a 200-nm-thick free-standing Si membrane using a combination of electron-beam lithography, reactive ion etching and wet etching (see SEM image in Fig. 5c).

Numerical simulations. The LDOS of the structure has been calculated by three-dimensional finite-difference time-domain methods, by using the commercial software FDTD Solutions from Lumerical Solutions. LDOS maps are obtained by probing the structure with a *z*-aligned electrical point dipole at a height of 1 nm above the structure and by recording the emitted power as a function of the dipole position and of its emission frequency. The resulting LDOS maps are normalized by the LDOS simulated for a homogeneous slab.

Received 4 March 2012; accepted 17 July 2012; published online 19 August 2012

References

1. Purcell, E. M. Spontaneous emission probabilities at radio frequencies. *Phys. Rev.* **69** 681 (1946).
2. John, S. Strong localization of photons in certain disordered dielectric superlattices. *Phys. Rev. Lett.* **58,** 2486–2489 (1987).
3. Garcia, P. D., Sapienza, R., Froufe-Pérez, L. & López, C. Strong dispersive effects in the light-scattering mean free path in photonic gaps. *Phys. Rev.* **79,** 241109(R) (2009).
4. Badolato, A. *et al.* Deterministic coupling of single quantum dots to single nanocavity modes. *Science* **308,** 1158–1161 (2005).
5. Englundet, D. *et al.* Controlling the spontaneous emission rate of single quantum dots in a 2D photonic crystal. *Phys. Rev. Lett.* **95,** 013904 (2005).
6. Curto, A. G. *et al.* Unidirectional emission of a quantum dot coupled to a nanoantenna. *Science* **329,** 930–933 (2010).
7. Akahane, Y., Asano, T., Song, B. & Noda, S. High-Q photonic nanocavity in a two-dimensional photonic crystal. *Nature* **425,** 944–947 (2003).
8. Kimble, H. J. The quantum internet. *Nature* **453,** 1023–1030 (2008).
9. Michaelis, J., Hettich, C., Mlynek, J. & Sandoghdar, V. Optical microscopy using a single-molecule light source. *Nature* **405,** 325–328 (2000).
10. Kuehn, S., Hettich, C., Schmitt, C., Poizat, J-P. & Sandoghdar, V. Diamond colour centres as a nanoscopic light source for scanning near-field optical microscopy. *J. Microsc.* **202,** 2–6 (2001).
11. Frimmer, M., Chen, Y. & Koenderink, A. F. Scanning emitter lifetime imaging microscopy for spontaneous emission control. *Phys. Rev. Lett.* **107,** 123602 (2011).
12. Taminiau, T. H., Stefani, F. D., Segerink, F. B. & van Hulst, N. F. Optical antennas direct single-molecule emission. *Nature Photon.* **2,** 234–237 (2008).
13. Englund, D. *et al.* Deterministic coupling of a single nitrogen vacancy center to a photonic crystal cavity. *Nano Lett.* **10,** 3922–3926 (2010).
14. Colas des Francs, G., Girard, C., Weeber, J. & Dereux, A. Relationship between scanning near-field optical images and local density of photonic states. *Chem. Phys. Lett.* **345,** 512–516 (2001).
15. Vignolini, S. *et al.* Polarization-sensitive near-field investigation of photonic crystal microcavities. *Appl. Phys. Lett.* **94,** 163102 (2009).
16. De Wilde, Y. *et al.* Thermal radiation scanning tunnelling microscopy. *Nature* **444,** 740–743 (2006).
17. Takeuchi, K. & Yamamoto, N. Visualization of surface plasmon polariton waves in two-dimensional plasmonic crystal by cathodoluminescence. *Opt. Express* **19,** 12365–12374 (2011).
18. García de Abajo, F. J. Optical excitations in electron microscopy. *Rev. Mod. Phys.* **82,** 209–275 (2010).
19. Kuttge, M. *et al.* Local density of states, spectrum, and far-field interference of surface plasmon polaritons probed by cathodoluminescence. *Phys. Rev. B* **79,** 113405 (2009).
20. Coenen, T., Vesseur, E. J. R. & Polman, A. Angle-resolved cathodoluminescence spectroscopy. *Appl. Phys. Lett.* **99,** 143103 (2011).
21. Kuttge, M., García de Abajo, F. J. & Polman, A. Ultrasmall mode volume plasmonic nanodisk resonators. *Nano Lett.* **10,** 1537–1541 (2009).
22. Yamamoto, N., Ohtani, S. & García de Abajo, F. J. Gap and Mie plasmons in individual silver nanospheres near a silver surface. *Nano Lett.* **11,** 91–95 (2011).
23. Bashevoy, M. V., Jonsson, F., MacDonald, K. F., Chen, Y. & Zheludev, N. I. Hyperspectral imaging of plasmonic nanostructures with nanoscale resolution. *Opt. Exp.* **15,** 11313–11320 (2007).
24. Vesseur, E. J. R. & Polman, A. Plasmonic whispering gallery cavities as optical nanoantennas. *Nano Lett.* **11,** 5524–5530 (2011).
25. López-García, M. *et al.* Enhancement and directionality of spontaneous emission in hybrid self-assembled photonic-plasmonic crystals. *Small* **6,** 1757–1761 (2010).
26. Notomi, M. Manipulating light with strongly modulated photonic crystals. *Rep. Prog. Phys.* **73,** 096501 (2010).
27. Vučković, J., Lončar, M., Mabuchi, H. & Scherer, A. Optimization of the *Q* factor in photonic crystal microcavities. *IEEE J. Quantum Electron.* **38,** 850–856 (2002).
28. Taminiau, T. H., Stefani, F. D. & van Hulst, N. F. Optical nanorod antennas modeled as cavities for dipolar emitters: Evolution of sub- and super-radiant modes. *Nano Lett.* **11,** 1020–1024 (2011).
29. Coenen, T., Vesseur, E. J. R. & Polman, A. Deep subwavelength spatial characterization of angular emission from single-crystal Au plasmonic ridge nanoantennas. *ACS Nano* **6,** 1742–1750 (2012).
30. Kuttge, M. *Cathodoluminescence Plasmon Microscopy*, Utrecht University, PhD thesis (2009).

Acknowledgements

We wish to thank P. de Roque, K. Kuipers, L. Novotny and J. García de Abajo for fruitful discussions and C. Dominguez for the growth of the Si_3N_4 membranes. This research was financially supported by the MICINN, programmes FIS2009-08203, CONSOLIDER CSD2007-046, RyC, Integrated nano and microfabrication Clean Room ICTS project, Fundació CELLEX, and the EU Project ERC and FP7 People. The work is part of the research programme of FOM, financially supported by NWO, and of the research programme NanoNextNL, funded by the Dutch Ministry of Economic Affairs.

Author contributions

All authors contributed extensively to the work presented in this paper. R.S. conceived the idea to carry out cathodoluminescence to probe the LDOS in photonic crystals; T.C. developed the angle-resolved cathodoluminescence imaging spectroscopy instrument. R.S. and T.C. performed the experiments. J.R., M.K. and R.S. fabricated the samples; R.S., T.C. and M.K. analysed the data; R.S. and M.K. performed the theoretical calculations. All authors contributed to the manuscript. N.F.v.H. and A.P. gave overall supervision.

Additional information

Supplementary information is available in the online version of the paper. Reprints and permissions information is available online at www.nature.com/reprints. Correspondence and requests for materials should be addressed to R.S.

Competing financial interests

The authors declare no competing financial interests.